Instrumented Compliant Wrist for Dexterous Robotic Interaction

Pascal Laferrière, Pierre Payeur, Rafael Toledo
School of Electrical Engineering and Computer Science
University of Ottawa
Ottawa, ON, Canada
[plafi092, ppayeur, rtole025]@eecs.uottawa.ca

***Abstract*—The design, assembly and implementation of a custom fabricated instrumented wrist aimed at supporting dexterous robotic interaction with live proximity and contact feedback is presented in this paper. Although comparable platforms have been conceived in the past, efforts have been made to reduce the complexity of the overall system with a focus on weight and cost reduction and the addition of a proximity detection feature. Design considerations are explored and compared to similar existing compliant wrists. An experimental characterization of the prototype is reported in the context of an integrated vision-guided robotic system. An evaluation of other possible applications, namely for mobile robotics, is also presented.**

Keywords—compliant wrist; dexterous robotics; touch feedback; proximity sensing; robot navigation

I. INTRODUCTION

In recent years, the role of modern robots has taken on a very different form than that of their early predecessors which were massively involved in industrial environments. While the latter could be easily programmed to perform repetitive tasks with a high degree of precision, as they benefited from structured environments and very few, if any, unknown variables, modern robots must deal with more complex scenarios. With advances in control theory and electronics, the possible applications for which robots are now being considered are innumerable, therefore requiring a change in the way more conventional problems are approached [1]. There is much work in the field of robotics whose aim is to find new ways of safely interacting with objects in unstructured and dynamic environments where people may or may not be present [2, 3]. Unstructured environments arise, in part, due to a lack of a priori knowledge of the surroundings or from the uncertainty present in localization methods and sensors on mobile platforms which cannot guarantee exact positions [4-6]. Another factor which contributes to this uncertainty is that not all objects have the same properties; some are malleable or deformable, others are solid or stiff while some are very fragile and require delicate handling. In many cases, if the robot is to operate in proximity to humans, their safety must also be considered. Compliance and back-drivability of actuators are often essential to achieving safer operation in situations with a human element. However, there is often a trade-off between repeatability and compliance. Depending on the scenario, more importance can be given to one factor over the other [7].

One of the goals of modern robotics is to increase functionality of devices beyond their current limitations. In the present work we attempt to incorporate a degree of compliance onto an initially non-compliant manipulator robot in the form of a compliant wrist device, allowing the robot to dynamically adapt to the surfaces it approaches or touches, but without requiring complex and high accuracy vision and range imaging feedback. To accommodate an inherent lack of precision in the vision stage, means of measuring the resulting deflections of the device when subjected to contact forces, as well as proximity detection elements, are embedded on the compliant wrist. The combination of both sensing mechanisms provides the necessary feedback to the robot controller for position control prior to and during contact with objects.

According to [8], the control of robotic manipulators can be divided into three modes of operation. The first is free-motion mode where the manipulator is moving through free space. With few external factors to manage during this type of control, the motion of manipulators can generally be stabilized via a common proportional plus derivative (PD) controller. The second is the impact or transition mode which is the moment that the manipulator comes into contact with an object. Finally, the third mode is the constrained motion mode where the manipulator must be controlled while maintaining contact with the desired object. The contact and proximity sensory information and compliance provided by the device introduced in this paper can allow manipulators to mitigate many problems which arise during the transition and constrained modes of operation [9].

In order for the device to provide a maximum flexibility and adaptation capability to various robotic platforms and tasks, the design requirements were to create a low cost, light weight and self-contained instrumented compliant wrist. The cost of existing manipulators is already somewhat restrictive and efforts should be made to reduce any additional costs incurred when modifying or expanding an existing platform. The low cost aspect was achieved by using widely available components such as mass produced microcontrollers and sensors. Moreover, most manipulators have a very limited payload and are unable to wield large end effectors. For example, the CRS F3 articulated robot used here to test the prototype has a nominal payload of only 3 kg. By fabricating a custom device made almost entirely from Delrin®, an acetal resin (polyoxymethylene) which is a thermoplastic with high stiffness and strength [10], significant weight reduction was achieved over an aluminum alternative.

978-1-4799-4926-7/14/$31.00 ©2014 IEEE

When looking to add custom tools to a manipulator, end effectors requiring dedicated connection ports can often hinder their integration into a system due to a lack of available connections. Also, certain tasks can require large ranges of movement, such as the turning of a screwdriver, where cables can interfere with the task and might require modifications in the control methods in order to accommodate the physical changes. The incorporation of a wireless transmission module, allowed for a self-contained unit requiring no direct external tethered connections. The conceptual design of the current prototype for the compliant mechanism is shown in Fig.1a and will be further detailed in the following sections.

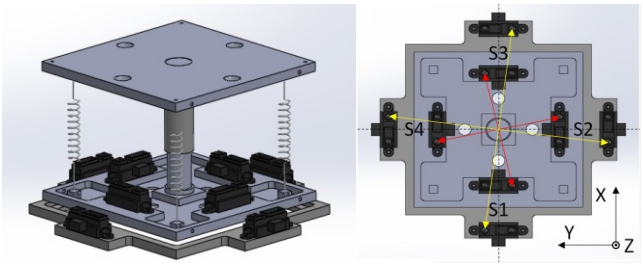

a) b)

Fig.1. a) Design of the instrumented wrist with spring loaded compliant plate, and b) dual sensory layers: internal (red) and external (yellow).

II. Related Work

The general concept of the proposed compliant wrist was inspired from previous works. Compliant wrist designs have been implemented for different applications such as surface mapping, contour following, automated assembly and haptic control [11-16]. In [11] and [12], the compliant wrist sensor is equipped with a tactile probe in order to obtain finer details of a contacted surface over the grosser estimate of surface position and orientation. 2D correlation techniques are used to stitch together surface images during sequential tactile exploration. The pose information generated by the compliant wrist structure is two rotations about the X and Y axes and a translation along the Z axis. The compliant structure however appears to experience a limited range of motion in both rotational and translation degrees of freedom due to the physical links joining the two plates. Several prototypes consisting of a much more complex design offering up to 6 degrees-of-freedom compliance are studied in [13-16], with provisions for measuring each of these 6 deflections. The passive compliance of the latter device is supplied by rubber elements which can be selected in order to produce a desired stiffness allowing for kinetic energy absorption during collision. The complexity of this design means that it doesn't lend itself well to modifications and also increases the cost of fabrication. The large number of moving parts also suggests that wear could be a factor in the long run. Both options also only offer a tethered connection to relay all of the sensory data which can easily interfere with the operation of a manipulator.

III. Motivation

Working with rigid robotic manipulators in unstructured environments can raise safety concerns especially in situations where human-robot interactions and the handling of fragile materials are a possibility. However, precise monitoring of the forces involved in the interaction is not always essential. The proposed instrumented compliant wrist is a cost effective alternative to classical hybrid control methods to complement vision-based guidance of robots. Hybrid control methods require the addition of force and torque measurement devices and major changes in the control paradigm of a robot, while the proposed strategy involves measuring geometrical transformations in between the end effector and the object with which the robot is, or about to be, interacting with. As a result, the control scheme of the robot does not require major modifications as feedback is provided in a form similar to what vision sensors already provide to support path planning [17, 18]. On the other hand, the added compliance offered by mounting the compliant wrist attachment onto an existing robotic platform can be a great asset in systems only equipped with visual feedback that provides information about the working environment but with relatively low accuracy.

Specific applications for this compliant wrist have been considered. One immediate application for which this design was achieved is that of a robotic system guided by a multi-modal sensing stage for automated vehicle inspection, as described in [19]. The robotic manipulator used in this system is expected to operate in an environment containing vehicles and their passengers while avoiding bodily injury to the passengers as well as causing no damage to the vehicles with which it comes into contact. Since neither compliance nor a purely vision-based system are sufficient to ensure safety, the system incorporates both a proximity and a contact sensory stage in addition to peripheral RGB-D visual information into its control loop. The goal is to increase the overall accuracy and dexterity of the end effector while interacting with the surface of a vehicle's bodywork, thereby increasing safety during the operation.

The sensors embedded on the compliant wrist allow for the combination of fast but low accuracy RGB-D data with proximity measurements during the approach, and eventually deviation monitoring of a compliant plate when in contact with the surface. This multi-sensory approach allows for the robot movements to be dynamically modified. Proximity sensing of surfaces also makes it possible to measure the exact location and orientation of surfaces occluded from the RGB-D vision sensor during preliminary visual inspection and shape estimation. It ensures a smooth transition from free-motion to transition, and up to constrained control modes [8]. Proximity detection also makes it trivial to predict when contact is about to occur, giving the robot controller ample time to adjust its trajectory for an optimal transition.

Another immediate application is the mounting of the proposed compliant structure onto mobile robot platforms to act as a form of agile bumper. Both the proximity and contact sensory information provided can help in collision avoidance as well as coarse mapping of boundaries. It can also help in tasks which involve multiple robots pushing objects collaboratively into desired directions, as each other's action can be monitored via the respective instrumented wrist mounted on every robot.

IV. Overall Design

Similar to the previously mentioned designs, at the core of the proposed compliant wrist assembly are two plates separated by components allowing for deflection of the upper compliant

plate under externally applied forces, as shown in Fig.1a. Instrumentation capable of dynamically measuring this deflection is embedded in the wrist (four internal sensors as shown in Fig. 1b). A second set of external sensors is added in the periphery of the bottom plate to measure the location of a surface before it actually touches the upper compliant plate, which provides the proximity sensory layer. The dual sensory layers provide the necessary measurements for fine tuning the approach of the robot while it is in close distance to the surface with which it is meant to interact but before the contact occurs. This strategy makes for a simpler solution than visual servoing as no computationally expensive image processing is required. Furthermore, the fine tuning of the robot interaction when contact is established is performed via real-time position and orientation feedback at the end effector level rather than force feedback, which allows to preserve the same control algorithm as when the more distant vision or RGB-D sensing is used. Specifics of the mechanical assembly, kinematic formulation, its operation and hardware considerations are given in the following subsections.

A. Mechanical Assembly

Starting at the base of the structure there is an attachment plate allowing the compliant wrist to be mounted to a variety of platforms. This attachment plate is fixed to the bottom of an enclosure used to house the electronics such as the microcontroller, wireless module, wiring and power source. This enclosure also provides a power switch and a USB access port allowing access to the microcontroller for reprogramming purposes or tethered operation, if required. The compliant mechanism, shown in Fig.1a, sits above the electronics enclosure. Four internal infrared (IR) sensors, shown in Fig. 1b, are mounted to the bottom plate positioned in such a way as to allow for direct measurement of the distance between the sensors and the movable upper plate. Fixed to the center of the bottom plate of the compliant mechanism is the bottom half of a hollow slide shaft housing a compression spring. The upper half of the shaft slides over the bottom half. This sliding motion provides the translational degree of freedom along the Z axis. A Teflon® (polytetrafluoroethylene or PTFE) ball is located at the tip of the upper half of the slide shaft providing a very low friction point of contact between the upper plate and the shaft, and giving the wrist its two rotational degrees of freedom, one about the X axis and another about the Y axis. Four extension springs join the four corners of the top and bottom plates keeping the upper plate in contact with its pivot point and adding stiffness to the wrist. The combination of opposing forces from both the compression and extension springs maintain the wrist in an equilibrium and tensioned state. Surrounding the base plate is a secondary sensor attachment plate to which an additional four IR sensors are mounted. These sensors allow the compliant wrist to detect external objects in proximity of the wrist along the same direction of the center shaft.

B. Kinematic Formulation

The design of the proposed compliant wrist provides for a simple kinematic representation of the device with 3 degrees of freedom. As mentioned in the previous section, the device employs two independent sets of four IR sensors. Both sets of sensors operate in the same fashion and are capable of generating similar distance information from their respective anchor points. However, the way in which the distance information is interpreted is dependent on the sensory layer considered. The internal sensors are used for upper plate deflection measurements. Therefore, the representation involves only two rotations and one translation measurements to completely describe the detected movement of the upper plate since the surface of the upper plate is uniformly planar.

Fig. 1b shows how both sets of sensors are organized with respect to the assigned reference frame. The reference frame has its origin located in the center of the sliding shaft, corresponding to the intersection between all red and yellow arrows. The extraction process of the rotation and translation parameters and of the normal vectors relies solely on distance measurements obtained from the IR sensors. Each rotation angle is calculated from the distance measurements of two IR sensors aligned along a particular axis. The rotation about the X axis is extracted from the distances measured by the two sensors aligned along the Y axis, and the rotation about the Y axis is extracted from the distances measured by the two sensors aligned along the X axis. By taking the arctangent of a right angle triangle whose vertical side is the difference in distance measurements of the two sensors on that axis with a base whose length is equal to the distance that separates the two sensors, the desired angle is obtained. An example of how the rotation angle about the Y axis is calculated, using the distances measured from two sensors aligned along the X axis, is given on the right of Fig. 2, assuming an in-between sensor distance of W. Rotations can be calculated according to Eq. (1) and (2) where S indicates a sensor distance, the subscripted letters denote the axis of alignment and the positive or negative signs denote on which side of the center of the axis these sensors are positioned.

$$R_X = \beta = atan2(S_{Y+} - S_{Y-}, W) \tag{1}$$

$$R_Y = \alpha = atan2(S_{X-} - S_{X+}, W) \tag{2}$$

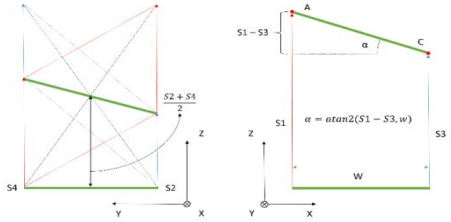

Fig. 2. Estimation of translation (left) and rotation (right) of the upper plate.

The translation along the Z axis is also obtained from the distance measurements of two sensors aligned along a particular axis. By taking the average of both distance measurements we can find the distance between the centers of the upper and lower plates. This is possible due to the symmetry of the sensor placement. Eq. (3) defines how the translation is calculated using the distances measured from two opposite sensors. An example is given on the left side of Fig. 2. Either pair of sensors along an axis can provide an estimate of the translation; however, the value will only be the same for both pairs if the surface is planar as seen by all four sensors in the set. This approach is therefore valid for the internal set of sensors that measure the deviation of the upper plate.

$$T_z = \frac{S_{X-} + S_{X+}}{2} = \frac{S_{Y-} + S_{Y+}}{2} \tag{3}$$

The relationship between the bottom plate (considered static from the point of view of the instrumented wrist) and the compliant upper plate can be represented as a 3D homogeneous transformation matrix, whose parameters depend on the four internal distance measurements, represented as A, B, C, and D in Fig. 3.

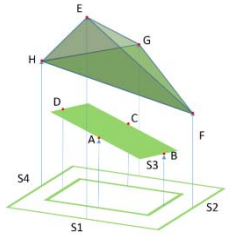

Fig. 3. Extracted distance measurements from internal and external sensors.

The equivalent homogeneous transformation, $Q_{compliant/effector}$, between the two plates is defined as follows:

$$Q_{compliant/effector} = \begin{bmatrix} \cos\alpha & 0 & \sin\alpha & 0 \\ \sin\beta\sin\alpha & \cos\beta & -\sin\beta\cos\alpha & 0 \\ -\cos\beta\sin\alpha & \sin\beta & \cos\beta\cos\alpha & \frac{B+D}{2} \\ 0 & 0 & 0 & 1 \end{bmatrix} \quad (4)$$

where $\beta = atan2(^{D-B}/_{W})$ and $\alpha = atan2(^{A-C}/_{W})$.

For proximity measurements that involve external object detection, it cannot be assumed that the objects encountered will be devoid of curvature or deformations. As shown in Fig. 3, points E, F, G and H are distances measured between the external sensors and objects in proximity of the device. In this case, the extraction of additional parameters provides a better representation of the encountered object's surface. These additional parameters come in the form of four normal vectors, which makes the estimation slightly more elaborate.

A plane can be described in several ways: a normal vector to the plane, a group of three points which lie on the plane, or similarly, two vectors which lie on the plane. Each of these concepts is used to generate four normal vectors corresponding to four distinct planes in three dimensional space. Given that there are four sensors in the external sensory layer, four points in three dimensions are obtained. Since only three points are required for describing a plane, four separate three-point groupings can be formed, which describe four possibly different planes each with its own normal. Referring to Fig. 1b, the four possible combinations of three sensors are (S4, S1, S2), (S1, S2, S3), (S2, S3, S4) and (S3, S4, S1), where each sensor, S#, corresponds to a point in space, and where the X and Y components of the points correspond to the known (by construction) X and Y coordinates of the sensor on the reference (bottom) plane, and the Z component corresponds to the respective measured distances by the sensor. The next step towards obtaining the normal vectors describing each potential plane on a distant object is to take the cross product of the two vectors obtained from the vector differences between two sensor pairs. In the general form, this corresponds to:

$$\overrightarrow{N_n} = \overrightarrow{S_n S_{n+1}} \times \overrightarrow{S_n S_{n-1}} \quad (5)$$

where *n* corresponds to any of the four external sensors, *n+1* corresponds to the next sensor in the group, and *n-1* corresponds to the previous sensor, each assembly being selected among the four groups of three sensors listed above. Combining the resulting four normal vectors with the original distance measurements allows the estimation of the overall surface orientation and curvature to be refined by creating multi-faceted representations of detected objects.

C. System Operation

The system developed is summarized in Fig. 4. The objects contoured by solid lines represent physical hardware and peripheral devices while dashed lines represent the implemented software components. The microcontroller is at the core of the compliant wrist system. The latter is represented in software by its own class which captures the physical aspects of the compliant wrist device such as the location of each IR sensor, the voltage measurements acquired from the IR sensors and the corresponding distances to those voltage measurements. This part of the system is also responsible for manipulating the distance measurements to obtain the translation along Z, the rotations about the X and Y axes from each sensor set, as well as the four separate normal vectors.

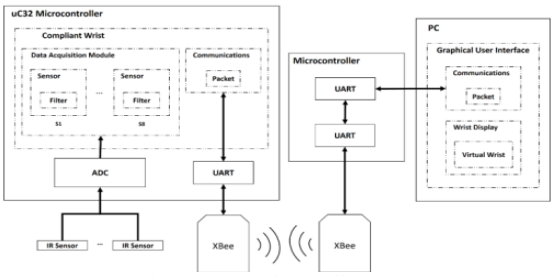

Fig. 4. System design diagram.

The data acquisition module is responsible for controlling the sampling rate of the analog-to-digital conversion (ADC) peripheral onboard the microcontroller to which the eight individual IR sensors are connected. It contains buffers for storing the incoming samples of the ADC and digital filters for additional signal processing prior to output generation.

All of the information gathered from the sensors, i.e. the raw sensor voltages, converted sensor distances, rotations, translations and normal vectors, is made available to external sources, such as the robot controller. The microcontroller used includes two universal asynchronous receiver-transmitters, one of which is connected to an XBee radio module.

The right portion of the diagram in Fig. 4 illustrates the setup for the visualization platform developed to aid in testing. It comprises of a personal computer equipped with a similar microcontroller and another XBee radio module giving it the ability to wirelessly communicate with the microcontroller located onboard the compliant wrist. A graphical user interface allows for the modification of settings of the software components in the compliant wrist and also provides a means of actively visualizing the operation of the compliant wrist.

D. Electronics and Signal Processing

The computing power of the instrumented compliant wrist is provided via a chipKIT uC32™ prototyping platform which has at its core a Microchip® PIC32MX340F512H microcontroller capable of operating at 80 MHz. The distance measurements allowing for deflection calculation are obtained via eight Sharp GP2Y0A41SK0F IR Range Sensors [20], which are operational over a range of 4 to 30 cm. Wireless communications is achieved with the use of a pair of Digi International XBee S1 radios and an additional microcontroller

equipped with UARTs capable of relaying the received information to a workstation, PC or robot controller.

The IR sensors are connected directly to the analog inputs of the microcontroller without any analog anti-aliasing filters. The IR sensor has an upper limit of roughly 80 Hz for the update frequency of the sensor's output [20]. The computing speed of the microcontroller allows the use of oversampling to minimize aliasing of the input signal. Signal conditioning is performed through the use of unity gain digital FIR filters obtained from the windowed sinc method as described in [21].

V. Compliant Wrist Experimental Characterisation

A physical prototype of the compliant wrist has been built, as shown in Fig. 5. The physical properties of the assembly and of the embedded sensors are analyzed in this section in order to determine the compliant wrist characteristics.

Fig.5.Prototype of the instrumented compliant wrist.

A. Measurement Precision

The ADC onboard the microcontroller provides a 10-bit resolution and therefore 1024 discrete voltage levels between 0 and 3.3V which is the default operating range of the device. This means that the smallest voltage change which can be detected, and therefore the maximum sensitivity of any sensor is approximately 0.0032V. Due to the shape of the characteristic voltage/distance curve provided in [20], a nonlinear relationship is obtained, leading to varying distance resolutions over the operational range of the sensor.

Considering extracted pairs of data points from [20] in Table 1, the theoretical expected resolutions in the given ranges of distance is established by calculating the slope in between adjacent data (voltage versus distance) as follows:

$$Resolution = \frac{p_{v1} - p_{v2}}{p_{d1} - p_{d2}} \quad (6)$$

Table 1. Sensor calibration data pairs.

Distance (cm)	Voltage (V)	Distance (cm)	Voltage (V)
40.0	0.300	10.0	1.270
35.0	0.370	9.0	1.400
30.0	0.440	8.0	1.560
25.0	0.520	7.0	1.770
20.0	0.650	6.0	2.020
18.0	0.740	5.0	2.340
16.0	0.820	4.0	2.720
14.0	0.930	3.5	3.000
12.0	1.060	3.0	3.050

Toward the maximum range of operation, a distance variation from 40 cm to 35 cm corresponds to 70 mV change, representing 0.0014 V/mm. Given that the ADC resolution is larger than this value, the actual distance resolution in that region is approximately 2.3 mm. At the other end of the valid distance range, going from 5 cm to 4 cm, the theoretical resolution is 0.038 V/mm which results in an approximate distance resolution of 0.085 mm. The current prototype has the internal sensors separated by a distance, W, of 91.8 mm (external sensors are separated by a distance of 165.1 mm) leading to a worst possible angular sensitivity of 1.435 degree over the largest distances. In comparison, [15] reports worst-case accuracies of 0.6 mm for translation and 0.0099 radians (0.57º) for rotation. Resolutions are omitted in [11] for both the distance and rotation, stating only the operating ranges of ±10º for rotation about the X and Y axes and a 10 mm travel of the upper plate's center point with respect to the lower plate's center point.

B. Sensor Calibration

In a preliminary version, the generated voltages of the IR sensors were converted to distance values according to the response curve given in [20]. The conversion from voltage to distance for intermediate values was made with the use of the Catmull-Rom spline interpolation technique. However, when two sensors were positioned at equal distances from a planar surface it was found that there were some variations in the output signal between the two sensors resulting in different measured distances. Fig. 6 shows a comparison of the response of four different sensors obtained experimentally against the theoretical response curve provided in the sensor's data sheet. The sensor voltages generated at shorter distances tend to be greater than expected, while those generated at longer distances tend to be lower than expected with slight variations among the sensors. This experiment revealed that the distance/voltage relationship curve available in [20] does not guarantee sufficiently accurate results.

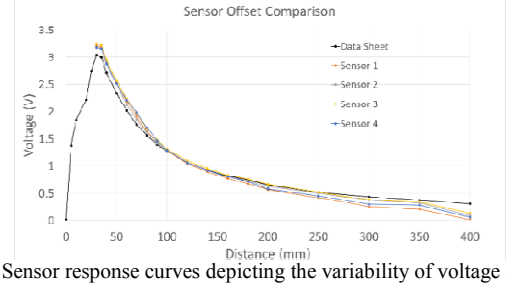

Fig. 6. Sensor response curves depicting the variability of voltage output compared to expected values for 4 distance sensors.

In order to improve the accuracy of the compliant wrist, both for proximity and contact interaction monitoring, a calibration procedure for the sensors was developed. A flat surface was mounted onto a 1D motorized track, equipped with encoders to provide accurate distance measurements to which the sensor outputs could be compared. Of the 23 provided distance/voltage pairs in the datasheet, 18 were found to be of practical use, namely the last 18, since the first 5 voltage values corresponding to distances below 3 cm cannot be discriminated from the voltage values corresponding to distances above 3 cm. These 18 calibration points are listed in Table 1. The track was positioned at each of the 18 distances and the actual voltage values provided by every individual sensor were measured and converted to distances. If the distance measured by the sensor did not match the distance measured by the track, the voltage output was offset until the distances were within a tolerance value supported by the 32 bit floating point numbers of the microcontroller. This procedure permitted to individually

compensate each of the individual sensor response curves to match a single desired response, which simplifies the implementation of the physical compliant wrist without introducing bias in the distance and transformation estimates.

VI. Discussion

The mechanical design intends to restrict motions which the embedded distance sensors are not able to measure, such as motions perpendicular to their sensing axis. The wrist relies on its central sliding shaft to prevent the compliant wrist from experiencing translations along both the X and Y axes. However, the central shaft's pivot point does not prevent rotations about the Z axis. Fortunately the distance and rotations measured are unaffected by this additional compliance. The current prototype offers only a limited range of motion due to the short length of the central shaft and the amount of tension provided by the extension springs. The conceptual model of the compliant wrist called for a shaft with an approximate travel of 5 cm. However, the actual forces imposed on the device by the four extension springs caused the center shaft to be compressed at an equilibrium distance less than the expected maximum travel.

Selecting IR sensors for supplying distance measurements was motivated by their low cost and longer detection range, as compared to most other types of proximity sensors. Both inductive and capacitive displacement sensors offer a high degree of precision but with limited ranges of detection [22, 23]. The use of linear potentiometers, as in [11], was also considered as they can easily be made for any desired operating range; however, the latter is directly linked to their cost, size and weight. Another drawback is that they require a physical link to the objects whose distance they measure, which prohibited the use of the wrist as a proximity sensor.

Currently, physical scalability of the device is restricted by the size of the IR sensors in use. The minimum operating distance and physical size of the sensors restrict the achievable size reductions. This in turn can pose limitations when trying to approach objects which are smaller in height or width than the separation distance between the external set of sensors or that possibly have sharp curvatures.

VII. Conclusion

This paper reports on the design and initial implementation of a standalone instrumented compliant wrist which can be easily integrated into a variety of systems such as robotic manipulators or mobile platforms to provide live feedback about the approach of an object by a robot and to help closely control the interaction with a surface. The data acquired during preliminary evaluation of the wrist shows that the proposed design provides adequate resolution to warrant integration into existing robotic systems requiring compliance. The self-contained design combined with a wireless communication interface with the robot controller simplifies the integration process onto a variety of existing platforms.

Acknowledgments

The authors acknowledge the support toward this research from the Natural Sciences and Engineering Research Council of Canada via Strategic Project Grant no. STPGP 381229-09, and from Ontario Ministry of Training, Colleges and Universities via the Ontario Graduate Scholarship program.

References

[1] N. Tsagarakis, M. Laffranchi, B. Vanderborght, and D. Caldwell, "A Compact Soft Actuator Unit for Small Scale Human Friendly Robots," in Proc. of*IEEE Intl Conf. on Robotics and Automation*, pp. 4356-4362, 2009.

[2] M. Zinn, O. Khatib, B. Roth, and J. Salisbury, "Playing it Safe: A New Actuation Concept for Human-Friendly Robot Design," *IEEE Robotics & Automation Magazine*, vol. 11, no. 2, pp. 12–21, 2004.

[3] F. Pierrot, E. Dombre, E. Dégoulange, L. Urbain, P. Caron, S. Boudet, J. Gariépy, and J. Megnien, "Hippocrate: a Safe Robot Arm for Medical Applications with Force Feedback," *Medical Image Analysis*, vol. 3,no. 3, pp. 285–300, 1999.

[4] D. Katz, J. Kenney, and O. Brock, "How Can Robots Succeed in Unstructured Environments?," in *Proceedings of Robot Manipulation: Intelligence in Human Environments* at Robotics:Science and Systems, Zurich, Switzerland, 2008.

[5] S.Chitta, E. Jones, M. Ciocarlie and K. Hsiao,"Perception, Planning, and Execution for Mobile Manipulation in Unstructured Environments,"in *Special Issue on Mobile Manipulation: IEEE Robotics and Automation Magazine*,vol. 19, no 2, 2012.

[6] P. Hebert, N. Hudson, J. Ma, T. Howard, T. Fuchs, M. Bajracharya, and J. Burdick, "Combined Shape, Appearance and Silhouette for Simultaneous Manipulator and Object Tracking," in Proc. of *IEEE Intl Conf. on Robotics and Automation, pp. 2405-2412*, 2012.

[7] M. Quigley, A. Asbeck, and A. Ng, "A Low-Cost Compliant 7-DOF Robotic Manipulator," in *Proc. of IEEE Intl Conf. on Robotics and Automation, pp. 6051-6058*, 2011.

[8] T. A. Shirey, "Active and Passive Interaction Control for Robotic Manipulators." Ph.D. thesis, Florida State University, United States, 2004.

[9] J. Hyde and M. Cutkosky, "Controlling Contact Transition," *IEEE Control Systems Magazine*, vol. 14, no. 1, pp. 25-30, 1994.

[10] "Acetal Resin," available online: http://www.dupont.com/products-and-services/plastics-polymers-resins/thermoplastics/brands/delrin-acetal-resin.html, [May 28, 2014].

[11] E. Petriu, W.S. McMath, S.K. Yeung, and N. Trif, "Active Tactile Perception of Object Surface Geometric Profiles", *IEEE Trans. on Instrumentation and Measurement,* vol. 41, no. 1, pp. 87-92, 1992.

[12] P. Payeur, C. Pasca, A. Cretu and E. Petriu, "Intelligent Haptic Sensor System for Robotic Manipulation," *IEEE Transactions on Instrumentation and Measurement*, vol. 54, no 4, pp. 1583−1592, 2005.

[13] Y. Xu and R. P. Paul, "A Robot Compliant Wrist System for Automated Assembly," in *Proc. of IEEE Intl Conf. on Robotics and Automation*, pp. 1750-1755, 1990.

[14] T. Lindsay and R. P. Paul, "Improved Instrumented Compliant Wrist Design," Techincal Report MS-CIS-92-77, GRASP Lab 334, University of Pennsylvania, 1992.

[15] T. S. Lindsay, P. R. Sinha, and R. P. Paul, "An Instrumented Compliant Wrist for Robotics Applications," in *Proc. IEEE Int. Conf. Robotics and Automation*, pp. 648-653, 1993.

[16] P. R. Sinha , Y. Xu , R. K. Bajcsy and R. P. Paul "Robotic Exploration of Surfaces with a Compliant Wrist Sensor", *International Journal of Robotics Research*, vol. 12, no. 2, 1993.

[17] L. Deng, F. Janabi-Sharifi, and I. Hasanzadeh, "Comparison of Combined Vision/Force Control Strategies for Robot", in *Proc. of SPIE Intl Symp. on Optomechatronic Technologies: Optomechatronic Systems Control Conference*, pp.1-12, 2005.

[18] Y. Mezouar, M. Prats, and P. Martinet, "External Hybrid Vision/Force Control", in *Proc. of the Intl Conf. on Advanced Robotics*, 2007.

[19] R. Fareh, P. Payeur, D. Nakhaeinia, R. Macknojia, A. Chavez-Aragon, A.-M. Cretu, P. Lafferière, R. Laganière, R. Toledo, "An Integrated Vision-Guided Robotic System for Rapid Vehicle Inspection", in *Proc. of IEEE Intl Systems Conference*, pp. 446-451, 2014.

[20] Sharp, "Distance Measuring Sensor Unit," GP2Y0A41SK0F datasheet, Aug. 2013.

[21] S. W. Smith, "The Scientist and Engineer's Guide to Digital Signal Processing," 2nd ed., San Diego, CA: California Technical Publishing, 1999.

[22] "Proximity Sensors: the Differences Between the Four Main Types," Internet:http://machinedesign.com/sensors/proximity-sensors-compared-inductive-capacitive-photoelectric-and-ultrasonic, [May 29, 2014].

[23] J. Wilson, "Capacitive and Inductive Displacement Sensors," in *Sensor Technology Handbook*, 1st ed., J. Wilson, Burlington MA: Elsevier-Newnes, Dec. 2004, pp. 193-222.